



**HAL**  
open science

# Quantifying East Asian Summer Monsoon Dynamics in the ECP4.5 Scenario With Reference to the Mid-Piacenzian Warm Period

Yong Sun, Gilles Ramstein, Laurent Li, Camille Contoux, Ning Tan, Tianjun Zhou

► **To cite this version:**

Yong Sun, Gilles Ramstein, Laurent Li, Camille Contoux, Ning Tan, et al.. Quantifying East Asian Summer Monsoon Dynamics in the ECP4.5 Scenario With Reference to the Mid-Piacenzian Warm Period. *Geophysical Research Letters*, 2018, 45 (22), pp.12,523-12,533. 10.1029/2018GL080061 . hal-02412922

**HAL Id: hal-02412922**

**<https://hal.science/hal-02412922>**

Submitted on 16 Dec 2019

**HAL** is a multi-disciplinary open access archive for the deposit and dissemination of scientific research documents, whether they are published or not. The documents may come from teaching and research institutions in France or abroad, or from public or private research centers.

L'archive ouverte pluridisciplinaire **HAL**, est destinée au dépôt et à la diffusion de documents scientifiques de niveau recherche, publiés ou non, émanant des établissements d'enseignement et de recherche français ou étrangers, des laboratoires publics ou privés.



**RESEARCH LETTER**

10.1029/2018GL080061

**Key Points:**

- A comparison of summer monsoon dynamics over East Asia for the mid-Piacenzian and the ECP4.5 scenario reveals both large-scale similarities and regional differences
- Large-scale similarity in moisture transport under thermal control and regional differences in vertical motion regulated by moist static energy
- Negligible effect of slight topographic difference on regional precipitation

**Supporting Information:**

- Supporting Information S1
- Figure S1

**Correspondence to:**

Y. Sun,  
sunyong@mail.iap.ac.cn

**Citation:**

Sun, Y., Ramstein, G., Li, L. Z. X., Contoux, C., Tan, N., & Zhou, T. (2018). Quantifying East Asian summer monsoon dynamics in the ECP4.5 scenario with reference to the mid-Piacenzian warm period. *Geophysical Research Letters*, 45, 12,523–12,533. <https://doi.org/10.1029/2018GL080061>

Received 16 AUG 2018

Accepted 1 NOV 2018

Accepted article online 6 NOV 2018

Published online 28 NOV 2018

# Quantifying East Asian Summer Monsoon Dynamics in the ECP4.5 Scenario With Reference to the Mid-Piacenzian Warm Period

Yong Sun<sup>1,2</sup> , Gilles Ramstein<sup>2</sup>, Laurent Z. X. Li<sup>3</sup>, Camille Contoux<sup>2</sup>, Ning Tan<sup>4</sup>, and Tianjun Zhou<sup>1</sup>

<sup>1</sup>State Key Laboratory of Numerical Modeling for Atmospheric Sciences and Geophysical Fluid Dynamics, Institute of Atmospheric Physics, Chinese Academy of Sciences, Beijing, China, <sup>2</sup>Laboratoire des Sciences du Climat et de l'Environnement, LSCE/IPSL, CEA-CNRS-UVSQ, Université Paris-Saclay, Gif-sur-Yvette, France, <sup>3</sup>Laboratoire de Météorologie Dynamique, CNRS, Sorbonne Université, Ecole Normale Supérieure, Ecole Polytechnique, Paris, France, <sup>4</sup>Key Laboratory of Cenozoic Geology and Environment, Institute of Geology and Geophysics, Chinese Academy of Sciences, Beijing, China

**Abstract** The mid-Piacenzian (~3.3–3.0 Ma), which was characterized by high  $p\text{CO}_2$  (~400 ppm) and global surface air temperatures that were 1.84–3.60 °C above pre-Industrial levels, provides clues to the likely changes in atmospheric dynamics in a future climate affected by anthropogenic warming, although its suitability as an analogue of the future climate has yet to be assessed. This study investigates the extent to which the dynamics of the East Asian summer monsoon during the mid-Piacenzian can aid our understanding of East Asian summer monsoon behavior in the Extended Concentration Pathway version 4.5 scenario, using water vapor and moist static energy equations. The temperature-dependent large-scale moisture transport explains the similar pattern of precipitation increase in the two climates, whereas regional patterns of vertical motion differ significantly. Two of the main terms of the moist static energy equation control the changes in regional dynamics relative to the pre-Industrial period. These terms relate to zonal advection of stationary eddy dry enthalpy by the mean zonal wind and meridional stationary eddy velocity over East Asia. Topographic differences between the two cases have a negligible effect on regional precipitation.

**Plain Language Summary** The mid-Piacenzian (~3.3–3.0 Ma, mid-Pliocene warm period) is the most recent warm period in Earth's history, characterized by high  $p\text{CO}_2$  levels (~400 ppm) and global warming (increase of 1.84–3.60 °C above pre-Industrial levels). Thus, it is of interest to compare this period with atmospheric dynamics responses to anthropogenic warming in a future climate, especially in terms of the monsoon. This study investigates the extent to which the dynamics of the East Asian summer monsoon during the mid-Piacenzian aid our understanding of the future behavior of the monsoon according to the Extended Concentration Pathway version 4.5 scenario. The analyses are based on water vapor and moist static energy equations. It is shown that increases in large-scale moisture transport under thermal control in the two warm climates enhance East Asian summer monsoon precipitation. Regional differences in East Asian summer monsoon precipitation arise from different contributions of dynamic processes, primarily zonal warm advection by zonal wind and meridional stationary eddy velocity. Topographic differences between the two cases have a negligible effect on regional precipitation.

## 1. Introduction

The mid-Piacenzian (~3.3–3.0 Ma) was the most recent warm period in Earth's history, with global mean surface air temperature estimated to have been 2–3 °C higher than pre-Industrial (PI) levels (Dowsett et al., 2013; Haywood et al., 2013; Salzmann et al., 2013). The geological conditions of the Earth during the mid-Piacenzian were similar to those of today (Haywood et al., 2011), including  $\text{CO}_2$  levels (Haywood et al., 2016). The mid-Piacenzian warming, which resulted in sea level rise (Miller et al., 2012) and ice sheet melting (Hill et al., 2007), is a potential analogue of future anthropogenic warming under increased greenhouse gas (GHG) emissions (Jansen et al., 2007).

The large-scale features of the mid-Piacenzian climate have been investigated in the framework of the Pliocene Model Intercomparison Project Phase 1 (PlioMIP1; Haywood et al., 2013). The global mean annual surface air temperature shows a 1.84–3.60 °C increase compared with PI values, with prominent warming

©2018. The Authors.

This is an open access article under the terms of the Creative Commons Attribution-NonCommercial-NoDerivs License, which permits use and distribution in any medium, provided the original work is properly cited, the use is non-commercial and no modifications or adaptations are made.

in high-latitude regions. An increase in GHGs played a dominant role in the tropical warming relative to PI, and surface albedo decrease was the dominant driver of the significant high-latitude warming and polar amplification compared with PI (Hill et al., 2014).

Features of regional climate (e.g., the monsoon, tropical atmospheric circulation, and Antarctic deep water) showed obvious responses to the mid-Piacenzian warming (Corvec & Fletcher, 2017; Haywood et al., 2013; Li et al., 2018; Sun et al., 2013; Zhang et al., 2009; Z. Zhang et al., 2013). The East Asian summer monsoon (EASM) in PlioMIP1 was characterized by a strengthening of the monsoon circulation and an increase in monsoon precipitation (R. Zhang et al., 2013). The midlatitude westerlies, a basic component of the global atmospheric circulation, were shifted poleward (Li et al., 2015), which is consistent with a poleward shift in the Hadley cell boundaries during the mid-Piacenzian (Sun et al., 2013). Zhang et al. (2015) investigated the sensitivity of the EASM to boundary conditions and found that sea surface temperature, CO<sub>2</sub> concentration, and ice sheet extent were key factors in creating a warm and wet climate over East Asia during the mid-Piacenzian. However, the precise physical mechanisms controlling the variations in the EASM during the mid-Piacenzian remain unclear. An understanding of the underlying physical processes is important if the mid-Piacenzian is to be considered an analogue of future GHG-induced warming.

This study examines the EASM dynamics in past and future warm climates to assess the degree to which the mid-Piacenzian climate is a suitable analogue of future changes in the EASM under a warming climate. We pay particular attention to the underlying physical mechanisms by decomposing the overall changes in water vapor budget (mid-Piacenzian and Extended Concentration Pathway version 4.5 (ECP4.5) compared with PI) into thermodynamic and dynamic components.

## 2. Data and Methodology

### 2.1. Model and Experimental Description

The present study focuses on diagnoses of three simulations performed with the IPSL-CM5A-LR model (Dufresne et al., 2013), which is able to reproduce the modern EASM climate (Figure S1). A PI simulation with fixed CO<sub>2</sub> of 280 ppm serves as a reference for mid-Piacenzian and ECP4.5 simulations. The mid-Piacenzian simulation used the PlioMIP1 protocol (Contoux et al., 2012) and employed simple boundary conditions (Sohl et al., 2009). The continental configuration of the mid-Piacenzian was similar to that of the modern condition, but ice sheets were smaller, sea level was 25 m higher, and CO<sub>2</sub> was 405 ppm, similar to today levels. Note, however, that the GHG-induced current global warming level above PI is much weaker than in the mid-Piacenzian because slowly responding components of the climate system had attained equilibrium during the mid-Piacenzian (Lunt et al., 2009; Salzmann et al., 2009) but are in a transient state in the present climate. The mid-Piacenzian simulation was run for about 980 years, with the last 30 years used for our analysis.

The Extended Concentration Pathway (ECP) version 4.5 simulation is a future projection under the framework of the Coupled Model Intercomparison Project phase 5 (Meinshausen et al., 2011), with increases in GHGs perturbing radiative forcing by 4.5 W/m<sup>2</sup> in 2100 (compared with PI levels). This simulation was extended until 2300 with radiative forcing and GHG concentrations almost constant at 2100 values via a smooth transition toward GHG stabilization by 2150 (CO<sub>2</sub> level stabilized at 543 ppm; Meinshausen et al., 2011). The extra 150 years of the simulation (2150 to 2300) with constant forcings ensures that the atmospheric surface climate is in equilibrium. The mid-Piacenzian simulation includes tectonic changes superimposed on *p*CO<sub>2</sub> variation (Contoux et al., 2012), so it cannot be directly compared with the future transient climate. It is valid to compare the EASM dynamics of the mid-Piacenzian with the last 30 years (2271 to 2300) of the ECP4.5 simulation in which the atmospheric processes are in equilibrium. Details of the model and simulations are given by Contoux et al. (2012), Dufresne et al. (2013), Haywood et al. (2011), and Sun et al. (2013).

In addition to CO<sub>2</sub> levels, the topography differs between the two warm climates (Figure S2). To test whether the slightly different topography in the two cases has a significant influence on the EASM, a sensitivity experiment (TopoPlio) was carried out, restarted from the final state of our PlioMIP1 with the same topography as in the ECP4.5 scenario. The sensitivity simulation was run for 150 years and the final 30 years are used for analysis.

## 2.2. Diagnostic Methodology

To identify the physical processes associated with EASM precipitation in response to past and future warming, the following moisture budget equation is used:

$$P = E - \langle \omega \hat{\partial}_p q \rangle - \langle \vec{V}_H \cdot \nabla q \rangle - \langle q \cdot \nabla \cdot \vec{V}_H \rangle + Res, \quad (1)$$

where  $P$  is the precipitation,  $E$  is the evaporation,  $\omega$  is the vertical velocity at a constant pressure coordinate,  $q$  is the specific humidity,  $V_H$  is the horizontal wind, and  $Res$  is a residual term. The angle brackets indicate the vertical integral over the atmospheric column throughout the troposphere (Chou & Lan, 2012). The dominant factors responsible for the changes in EASM precipitation during the two warm climates are identified by calculating the difference in each term in equation (1) relative to PI conditions. The variation in vertical advection ( $-\langle \omega \hat{\partial}_p q \rangle$ ) can be further decomposed into a thermodynamic component ( $-\langle \bar{\omega} \hat{\partial}_p q' \rangle$ ) and a dynamic component ( $-\langle \omega' \hat{\partial}_p \bar{q} \rangle$ ), as follows:

$$-\langle \omega \hat{\partial}_p q \rangle' = -\langle \bar{\omega} \hat{\partial}_p q' \rangle - \langle \omega' \hat{\partial}_p \bar{q} \rangle. \quad (2)$$

The thermodynamic contribution to precipitation changes comes from changes in air water vapor content with unchanged vertical circulation, whereas the dynamic contribution indicates changes in vertical motion with unchanged air water vapor content (Chou & Lan, 2012). The prime denotes the differences between each of the two warm climates and PI, and the overbar indicates the PI climatology.

To further understand regional variations in vertical motion and their relation to EASM precipitation, we use the moist static energy (MSE) equation for relevant diagnostics of the monsoon dynamics (Chen et al., 2018; Chen & Bordoni, 2014a, 2014b; Sun et al., 2016; Yao et al., 2017). Here we extend its application to two different climates: the mid-Piacenzian and the ECP4.5 anthropogenic warming scenario. The MSE budget equation can be written as follows:

$$\langle \omega \hat{\partial}_p MSE \rangle = \overline{F^{net}} - \langle V \cdot \nabla E \rangle, \quad (3)$$

where the overbar indicates the time mean,  $\overline{F^{net}}$  is the net heat flux into the atmospheric column (turbulent fluxes and radiation), and  $E$  is the moist enthalpy. Given that MSE decreases with increasing pressure in the troposphere, regions where the right-hand sum is positive are associated with ascending motion (precipitation, if considering the water budget equation), while descending motion (aridity) is associated with a negative right-hand sum.

## 3. Results

### 3.1. Comparison of Precipitation Changes Between the Mid-Piacenzian and ECP4.5

The simulated precipitation in the mid-Piacenzian shows an increase over East Asia (Figure 1a, colored areas), which is consistent with the wetter conditions indicated by seven geologic records collated by R. Zhang et al. (2013), including six pollen records (Hao et al., 2012; Jiang & Ding, 2008; Li et al., 2004; Ma et al., 2005; Wu, 2001; Wu et al., 2007) and one fruit-seed record (Zhao et al., 2004). Moreover, increased precipitation during the mid-Piacenzian is a common feature of the majority of PlioMIP1 models (Figure S3). This consistency between model and proxy data across multiple models increases the reliability of estimated EASM precipitation changes during the mid-Piacenzian. A general increase in precipitation over East Asia is also observed in the ECP4.5 scenario for most of the Coupled Model Intercomparison Project phase 5 models (Figure S3). The precipitation increase in both cases indicates similarities between the two climates.

In addition to similarities, the mid-Piacenzian and ECP4.5 scenario show regional differences in terms of the increase in EASM precipitation. For example, land precipitation increases significantly in China during the mid-Piacenzian compared with the PI period, with the increase occurring in a band aligned southwest-northeast (Figure 1a), while oceanic precipitation shows significant increases in the future scenario relative to the PI period (Figure 1b). In detail, relative to the ECP4.5 scenario the mid-Piacenzian shows a significant increase in land precipitation over South China and a decrease in precipitation over the adjacent ocean (Figure 2a). The cause of this regional difference and the insignificant effect of the slight difference in topographic configuration on regional precipitation is clarified in following paragraph.

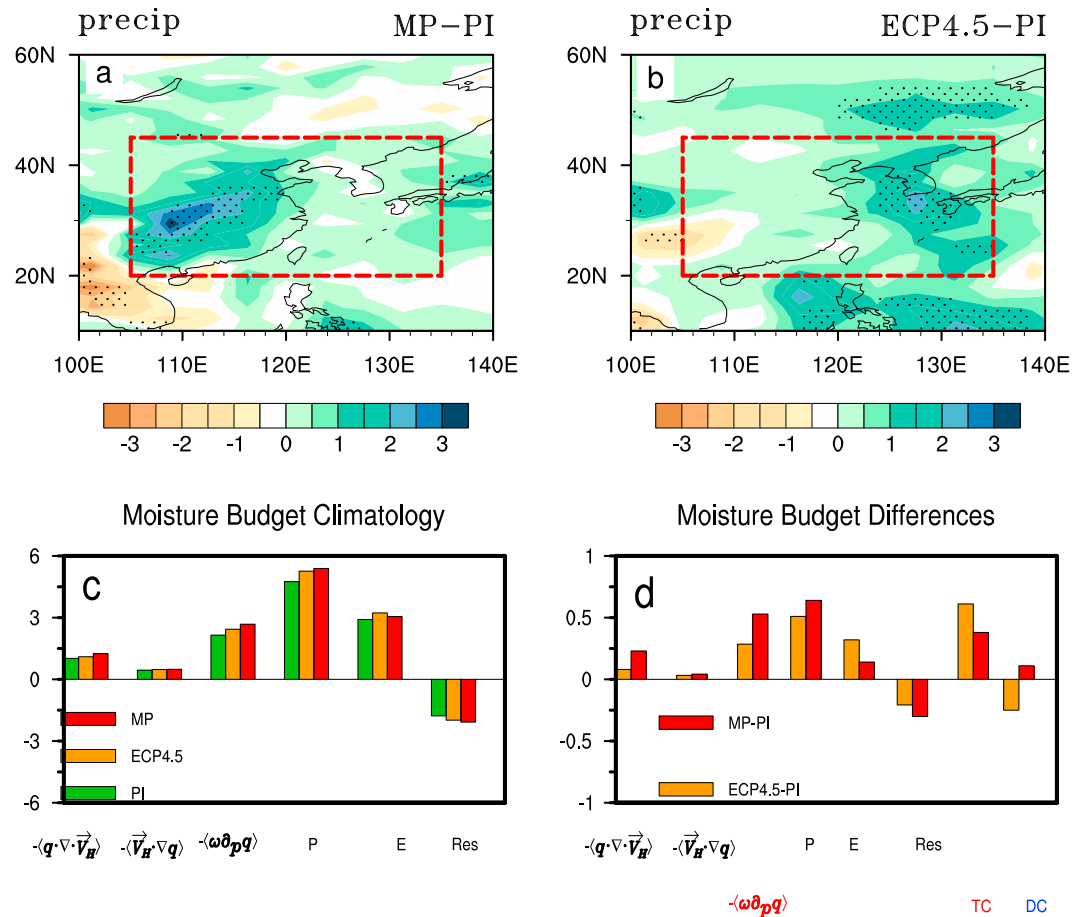


**Figure 1.** Spatial patterns of EASM precipitation changes relative to the PI period (units: mm/day) for (a) the mid-Piacenzian (MP) and (b) the ECP4.5 scenario. Relevant physical processes diagnosed by application of moisture budget analysis to (c) MP and (d) ECP4.5. The red rectangles in (a) and (b) indicate the East Asia domain (20°N–45°N, 105°E–135°E) used in this study. Dots in (a) and (b) denote statistical significance above the 1% level. In addition, TC (DC) in (d) indicates the thermodynamic (dynamic) contribution to equation (2).

Our sensitivity experiment shows that precipitation differences between TopoPlio and ECP4.5 (Figure 2b) are similar to those between the mid-Piacenzian and ECP4.5 (Figure 2a); that is, the slight topographic differences contribute little to the differences in regional rainfall patterns between the two warm climates (compare Figures 2a and 2b). The large differences in regional precipitation are likely to reflect the contrasting responses of regional monsoon dynamics to the warm equilibrium climate of the mid-Piacenzian and a future transient warming climate. Two mechanisms ( $\langle \bar{V}^* \rangle$  and  $-\left\langle [C_p \bar{U}] \cdot \frac{\partial T^*}{\partial x} \right\rangle$ ), identified as dominant fields for regional structures of the precipitation pattern in the warm climates (section 3.3.2), are used to understand the insignificant topographic effect on regional differences in EASM precipitation patterns. These effects are mainly regulated by  $\langle \bar{V}^* \rangle$ , as a significant increase in land precipitation is associated with southerly wind and a decrease in precipitation is associated with northerly wind over the adjacent ocean (Figures 2a and 2b). The term  $-\left\langle [C_p \bar{U}] \cdot \frac{\partial T^*}{\partial x} \right\rangle$  (Figures 2c and 2d) plays a smaller role in the “wetter land and drier ocean” precipitation distribution shown in Figures 2a and 2b. The mechanism by which  $\langle \bar{V}^* \rangle$  and  $-\left\langle [C_p \bar{U}] \cdot \frac{\partial T^*}{\partial x} \right\rangle$  regulate the regional precipitation is examined in detail in section 3.3.2.

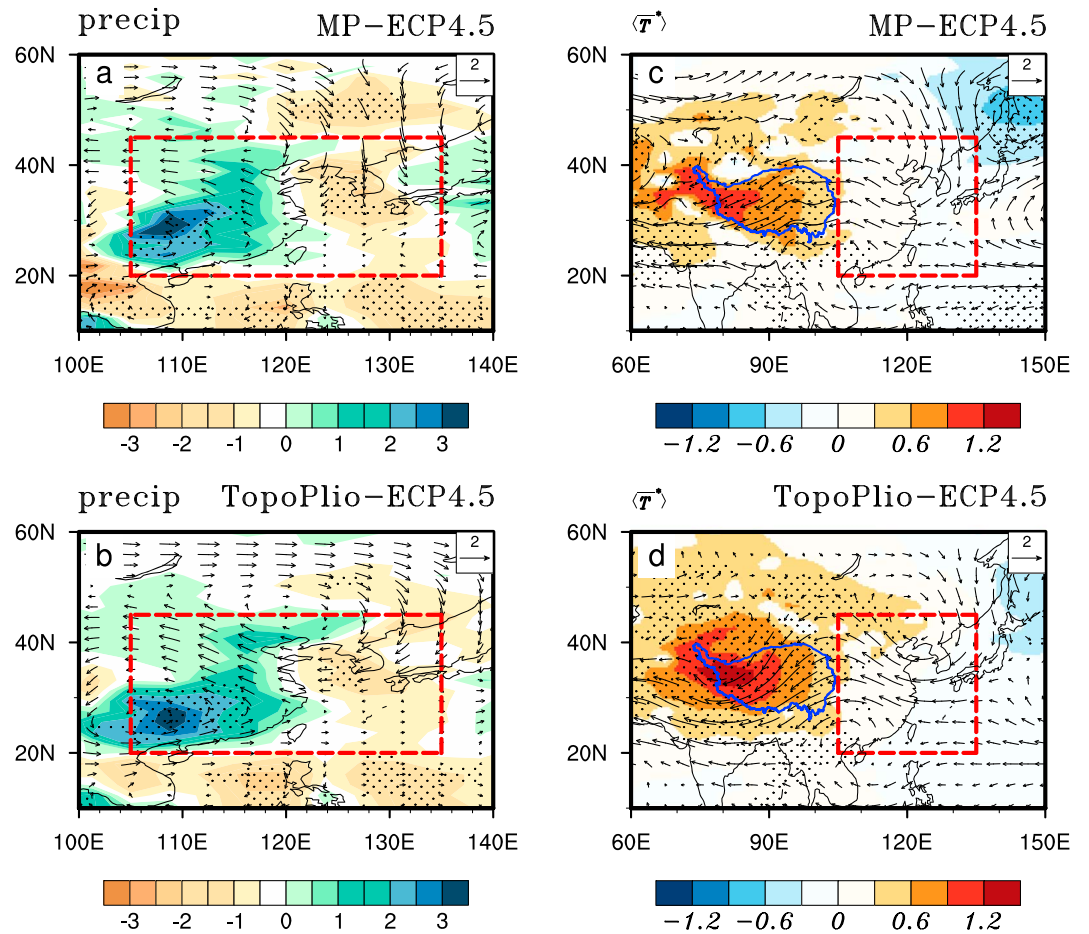


**Figure 2.** Regional pattern of precipitation difference (units: mm/day) (a) between MP and ECP4.5 and (b) between TopoPlio (MP experiment with the topography of ECP4.5) and ECP4.5. (c and d) The corresponding vertical integrals of stationary eddy circulation (vectors; units: m/s) and stationary eddy temperature (shading; units: °C). Dots indicate significance above the 1% level.

### 3.2. Physical Processes Revealed by Changes in the Water Vapor Budget

The moisture budget equation can help us to better understand EASM as it provides a way to decompose precipitation changes into different terms associated with different physical processes. We first examine the climatology of each term in equation (1) before applying it to changes in the mid-Piacenzian and ECP4.5 scenario. The results in Figure 1c are the regional average for the area indicated by the rectangle in Figure 1a. Precipitation occurs mainly due to the joint contribution of local evaporation and vertical advection of moisture (referred to as vertical moisture transport; Figure 1c). Moisture convergence and horizontal advection of moisture (referred to as horizontal moisture transport) play a secondary role (Figure 1c). In comparison with the PI period, the enhanced precipitation during the mid-Piacenzian is attributed mainly to an increase in vertical moisture transport (Figure 1d), whereas that in the ECP4.5 scenario is due largely to increases of local evaporation and vertical moisture transport. Of note, the atmospheric CO<sub>2</sub> concentration in ECP4.5 (543 ppm) is higher than that during the mid-Piacenzian (405 ppm), whereas the increase in EASM precipitation in ECP4.5 is much smaller than that during the mid-Piacenzian.

Because the vertical moisture transport term plays an important role in both climates, it is useful to decompose its changes into thermodynamic and dynamic components, and assess the relative contribution of each component. The thermodynamic terms in both warm climates are the dominant contributors to vertical moisture transport increase (Figure 1d). They essentially represent an increasing response of atmospheric water vapor to warming and show a larger contribution with higher CO<sub>2</sub> concentrations. In contrast, dynamic processes contribute differently to the vertical moisture transport in the two warmer climates (Figure 1d). The

dynamic term for the mid-Piacenzian has the same sign as vertical moisture transport and thus contributes positively to precipitation increase over the EASM domain. On the other hand, dynamic processes reduce upward vertical moisture transport under the ECP4.5 scenario and to some extent diminish the increase in projected EASM precipitation.

### 3.3. Physics of Thermodynamic and Dynamic Processes

Here we consider the physics of the thermodynamic and dynamic processes, and examine the meteorological conditions leading to precipitation. Obviously, the thermodynamic process is tied to moisture change (but constant large-scale atmospheric circulation), while the dynamic process captures the vertical motion related to monsoonal precipitation. We address the large-scale thermal control that produces the similar EASM precipitation changes of the two warm climates, and clarify the dynamic interpretation of regional differences in precipitation.

#### 3.3.1. Large-Scale Similarity of the Two Climates Under Thermal Control

As mentioned above, the strength of the large-scale moisture transport into the EASM domain is influenced by changes in the strength of the tropical atmospheric circulation and the atmospheric water vapor content. As the climate warms, the tropical atmospheric circulation weakens (not shown) and the atmospheric water vapor content increases (constrained by the Clausius-Clapeyron relation). Compared with the PI period (Figure S4a), increases in large-scale moisture transport are observed in both warm climates (Figures S4b and S4c). Therefore, the moisture flux increase results primarily from the increase in atmospheric vapor content. The increase in thermally controlled large-scale moisture transport is the large-scale background for the increase in EASM precipitation in both climates, which induces a large-scale similarity of the monsoonal climate over East Asia between the mid-Piacenzian and the ECP4.5 scenario.

#### 3.3.2. Regional Differences in Vertical Motion Regulated by MSE

In addition to the thermally controlled large-scale similarity of the two warm climates, regional differences in precipitation changes and their relation to vertical motion were described in section 3.2. The physical processes that affect regional vertical motion are further clarified by the MSE budget, as the vertical motion ( $\omega$ ) in the pressure coordinate is directly involved in the MSE balance (equation (3)).

##### 3.3.2.1. Regional Structures of Two Dominant Fields

A detailed analysis of the MSE budget (Sun et al., 2016) identifies the two dominant terms that affect the regional patterns of vertical motion change: the advection of stationary eddy (i.e., zonally varying time-mean)

dry enthalpy by zonal-mean flow ( $-\langle [C_p \bar{U}] \cdot \frac{\partial \bar{T}^*}{\partial x} \rangle$ ; Figures 3a and 3b) and the advection of zonal-mean dry

enthalpy by the meridional stationary eddy velocity ( $-\langle C_p \bar{V}^* \cdot \left[ \frac{\partial \bar{T}}{\partial y} \right] \rangle$ ; Figures 3c and 3d). The square brackets

indicate zonal averages, overbars the time mean, asterisks the deviation from the zonal average,  $C_p$  the specific heat at constant pressure,  $U$  the zonal velocity, and  $V$  the meridional velocity. We now compare the regional patterns of these terms between the mid-Piacenzian and the ECP4.5 scenario.

There are distinct differences in the structure of each dominant field in the two warm climates. For example, a

southwest-northeast trending structure of  $-\langle [C_p \bar{U}] \cdot \frac{\partial \bar{T}^*}{\partial x} \rangle$  is observed in the mid-Piacenzian (Figure 3a),

which is consistent with the southwest-northeast trending structure of precipitation anomalies during this period (Figure 1a). An east-west dipole structure with maximum anomalies over the Korean Peninsula and Kyushu (and the adjacent ocean) is seen in ECP4.5 (Figure 3b), which coincides well with the significant increase in future precipitation in this region (Figure 1b). There is also an east-west dipole structure of

$-\langle C_p \bar{V}^* \cdot \left[ \frac{\partial \bar{T}}{\partial y} \right] \rangle$  in the mid-Piacenzian (Figure 3c), which is consistent with the large increase in land

precipitation during the mid-Piacenzian and the decrease over adjacent ocean (Figure 1a). In contrast, a south-north dipole structure of this field is observed in ECP4.5 with negative anomalies occupying the EASM domain (Figure 3d). In general, the sum of the two dominant fields captures the regional structures of vertical motion related to precipitation changes in the two warm climates (Figures 3e and 3f).

The effect of  $\bar{F}^{\text{net}}$  during the mid-Piacenzian (compare Figures 3g and 3e) is negligible, but the involvement

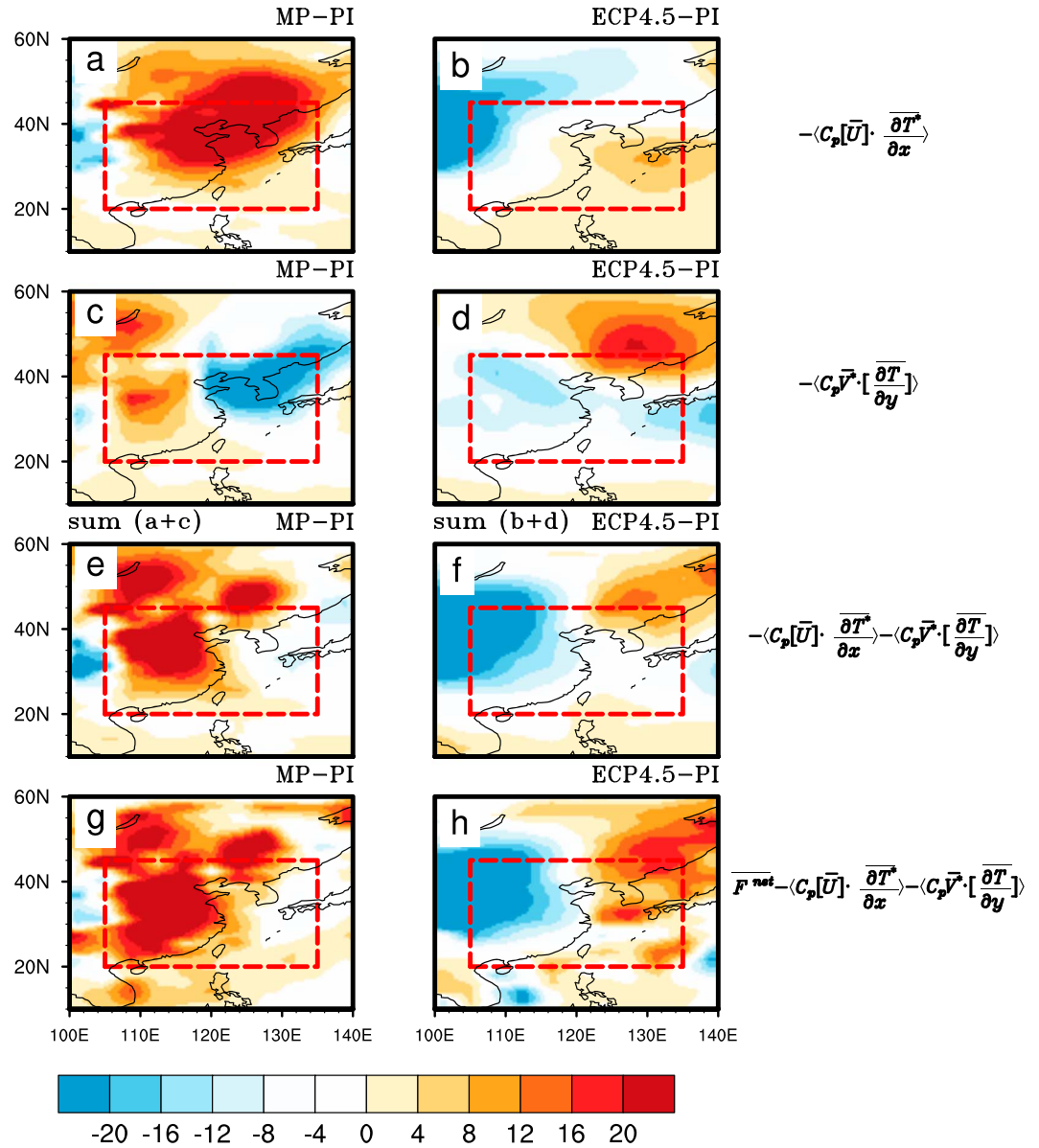


**Figure 3.** (top two rows) The two dominant terms controlling the MSE anomalies with respect to PI in (left) MP and in (right) ECP4.5. (first row) Advection of eddy dry enthalpy by the zonal-mean flow ( $W/m^2$ ). (second row) Advection of zonal-mean dry enthalpy by the meridional eddy velocity ( $W/m^2$ ). (third row) Sum of the first two terms. (fourth row) The  $\bar{F}^{net}$  changes involved in the sum ( $W/m^2$ ).

of  $\bar{F}^{net}$  in ECP4.5 results in enhanced local ascending motion over oceanic regions (compare Figures 3h and 3f).

### 3.3.2.2. Physical Interpretation of the Two Dominant Fields

Here we attempt to understand the different structures of the two major MSE terms in the two warm climates

and their relation to vertical motion. The effect of  $-\left\langle [c_p \bar{U}] \cdot \frac{\partial T^*}{\partial x} \right\rangle$  on vertical motion comes from the zonal

mean circulation acting on the zonal gradient of the stationary eddy air temperature  $\langle \bar{T}^* \rangle$ , which is a good indicator of the zonal thermal contrast over the EASM domain. Climatologically, the zonal thermal contrast results from the remarkably strong heating over the Tibetan Plateau and relatively weak warming over the adjacent ocean (Figure 4a, shading). This inhomogeneity, with the background mean zonal wind (Figure 4a, wind barbs), transports MSE into the region, inducing ascending motion and increasing

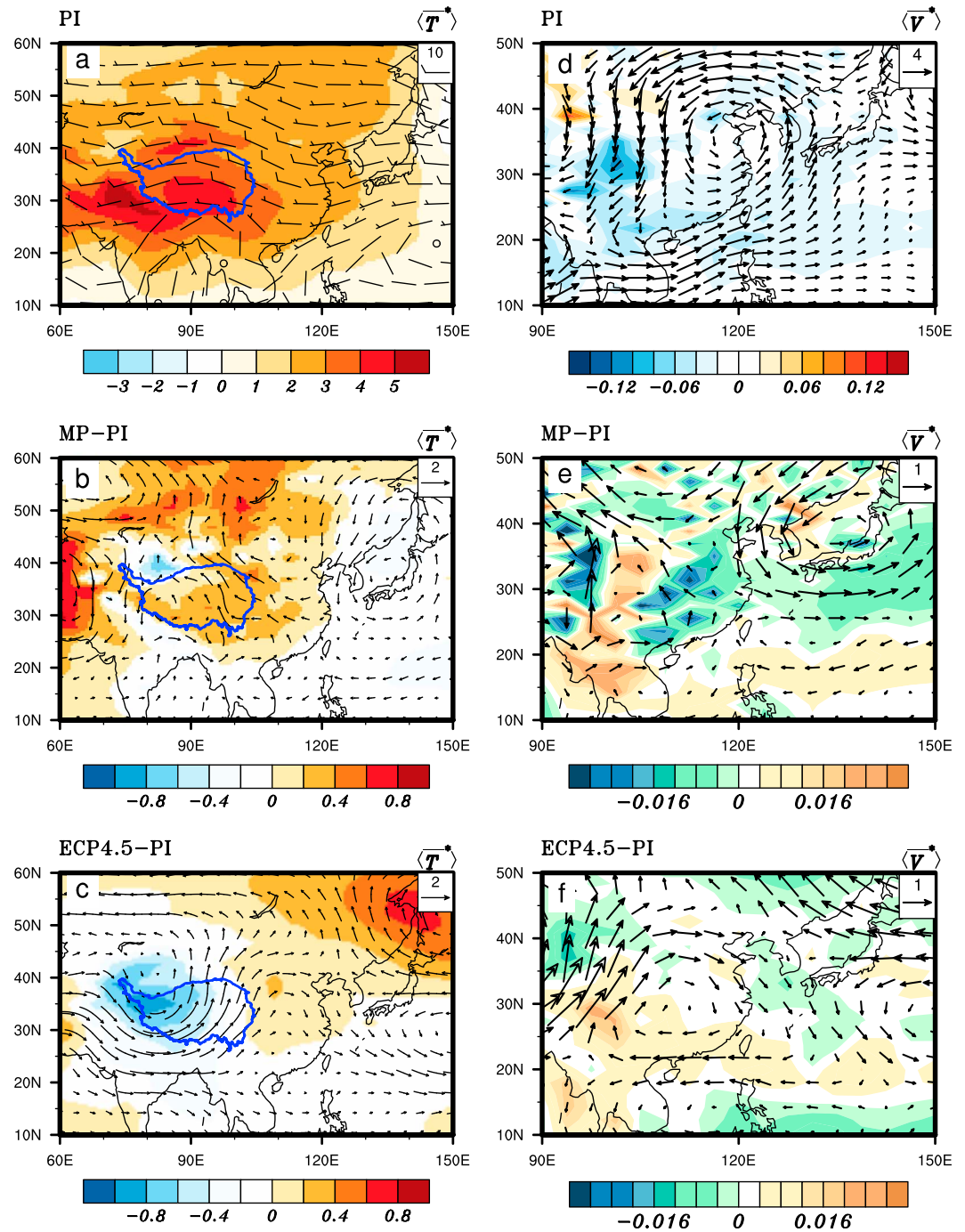


**Figure 4.** (left panel) Vertical integrals of horizontal circulation (wind bars) and (first row, left panel) stationary-eddy air temperature ( $\langle \bar{T}^* \rangle$ ; shading) and (first row, right panel) vertical integral of stationary eddy velocity ( $\langle \bar{V}^* \rangle$ ; vectors), superimposed with (first row, right panel) vertical integral of vertical motion (shading). Panels in the second and third rows show the differences, that is, (middle panel) MP-PI and (bottom panel) ECP4.5-PI.

precipitation. Generally speaking, we can deduce that ascending motion should occur when the zonal mean circulation transports anomalously warm air into a cold area.

Changes in  $\langle \bar{T}^* \rangle$  in the two warm climates are far from zonally uniform (Figures 4b and 4c), leading to an enhancement of zonal thermal contrast due to the warm Tibetan Plateau in the mid-Piacenzian (Figure 4b) and weakened land-sea thermal contrast in ECP4.5 due to a decrease in  $\langle \bar{T}^* \rangle$  over the Tibetan Plateau

(Figure 4c). The increase in land-sea thermal contrast strengthens the mid-Piacenzian EASM flow from ocean to land, and an anticyclone is observed over China (Figure 4b, vectors). The resulting westward and eastward warm advection by easterly and westerly winds on the southern and northern flanks of the anticyclone contributes to the tilted structure of  $-\left\langle [C_p \bar{U}] \cdot \frac{\partial \bar{T}^*}{\partial x} \right\rangle$  in the mid-Piacenzian (Figure 3a). In contrast, the weakening of the EASM in ECP4.5 is associated with warm advection by westerly anomalies from land to the adjacent ocean (Figure 4c, vectors), which contributes to the strong ascending motion over the ocean (Figure 3b). Further simplification identifies the meridional stationary eddy velocity  $\langle \bar{V}^* \rangle$  as the dominant component determining the spatial pattern of  $-\left\langle C_p \bar{V}^* \cdot \left[ \frac{\partial \bar{T}}{\partial y} \right] \right\rangle$ . Thus,  $\langle \bar{V}^* \rangle$  is used to illustrate the meridional eddy advection of temperature in relation to vertical motion. Again, to simplify, a northward anomalous circulation ( $\langle \bar{V}^* \rangle > 0$ ) implies ascending motion, and a southward anomalous circulation ( $\langle \bar{V}^* \rangle < 0$ ) implies descending motion.

In the PI climatology, northward stationary eddy circulation is generally found along the eastern flank of the anomalous cyclone over the EASM domain (Figure 4d, vectors), thereby inducing ascending motion by the northward transport of warm advection (Figure 4d, shading). Changes in  $\langle \bar{V}^* \rangle$  during the mid-Piacenzian show anomalous southerly flow from the low-latitude tropical ocean to South China that induces ascending motion in the region (Figures 3c and 4e). Anomalous southward advection from midlatitude regions to the eastern part of this warm advection suppresses the ascending motion over the Korean Peninsula and surrounding regions (Figure 4e). Therefore, the combination of northward and southward transports driven by  $\langle \bar{V}^* \rangle$  contributes to the dipole structure of  $-\left\langle C_p \bar{V}^* \cdot \left[ \frac{\partial \bar{T}}{\partial y} \right] \right\rangle$  in the mid-Piacenzian (Figure 3c).

In contrast, a general weakening of the stationary eddy circulation in the ECP4.5 scenario compared with PI leads to the anomalous northerlies observed over the EASM domain (Figure 4f, vectors), which induce descending motion anomalies and suppress the ascending motion over the EASM domain (Figure 4f, shading).

#### 4. Summary and Conclusions

This study assessed the extent to which the Pliocene warm climate provides clues to the response of regional monsoon climate to future anthropogenic warming. By comparing monsoon dynamics between the past (mid-Piacenzian) and future (ECP4.5) warm climates, we have observed similar EASM precipitation changes between the two climates and clarified the mechanisms controlling regional differences in precipitation structure. The key findings are summarized as follows:

1. East Asia is warmer and wetter than the PI period during the mid-Piacenzian and ECP4.5. In addition to an overall enhanced EASM in both climates, there are large differences in spatial patterns of EASM precipitation between the two warm climates, and these regional differences are not caused by the slight topographic difference between the two cases.
2. By analyzing the moisture budget and its different components, we were able to assess the physical processes controlling the EASM precipitation changes. Increases in large-scale moisture transport associated with greater moisture content in warmer air during the two warm climates resulted in enhanced EASM precipitation. Regional differences in EASM precipitation pattern result from different contributions of dynamic processes in the two warm climates.
3. An assessment of the MSE budget identified two dominant terms controlling dynamic processes:

$-\left\langle [C_p \bar{U}] \cdot \frac{\partial \bar{T}^*}{\partial x} \right\rangle$  represents the zonal stationary eddy air temperature advection via zonal mean zonal wind and  $\langle \bar{V}^* \rangle$  dominates the meridional temperature advection by the meridional stationary eddy velocity and contributes to vertical motion. The quite different structures of these two terms may explain the distinctive structures of regional precipitation in the two climates.

## Acknowledgments

We acknowledge the World Climate Research Program's Working Group on Coupled Modeling, which is responsible for Coupled Model Intercomparison Project, and we thank the climate modeling groups (listed in Figures S1 and S2 of this paper) for producing and making available their model output. This work was jointly supported by the National Natural Science Foundation of China (41661144009, 41505076), the China Scholarship Council, and the Chinese–French CAI YUANPEI Project. Appendix figures are available online (e.g., Figure S1 is the first figure in Appendix S).

## References

- Chen, J., & Bordoni, S. (2014a). Orographic effects of the Tibetan Plateau on the East Asian summer monsoon: An energetic perspective. *Journal of Climate*, *27*(8), 3052–3072. <https://doi.org/10.1175/jcli-d-13-00479.1>
- Chen, J., & Bordoni, S. (2014b). Intermodel spread of East Asian summer monsoon simulations in CMIP5. *Geophysical Research Letters*, *41*, 1314–1321. <https://doi.org/10.1002/2013gl058981>
- Chen, X. L., Wu, P. L., Roberts, M. J., & Zhou, T. J. (2018). Potential underestimation of future Mei-yu rainfall with coarse resolution climate models. *Journal of Climate*, *31*(17), 6711–6727. <https://doi.org/10.1175/JCLI-D-17-0741.1>
- Chou, C., & Lan, C.-W. (2012). Changes in the annual range of precipitation under global warming. *Journal of Climate*, *25*(1), 222–235. <https://doi.org/10.1175/JCLI-D-11-00097.1>
- Contoux, C., Ramstein, G., & Jost, A. (2012). Modelling the mid-Pliocene warm period climate with the IPSL coupled model and its atmospheric component LMDZ5A. *Geoscientific Model Development*, *5*(3), 903–917. <https://doi.org/10.5194/gmd-5-903-2012>
- Corvec, S., & Fletcher, C. G. (2017). Changes to the tropical circulation in the mid-Pliocene and their implications for future climate. *Climate of the Past*, *13*, 135–147. <https://doi.org/10.5194/cp-13-135-2017>
- Dowsett, H. J., Foley, K. M., Stoll, D. K., Chandler, M. A., Sohl, L. E., Bentsen, M., et al. (2013). Sea surface temperature of the mid-Piacenzian Ocean: A data-model comparison. *Scientific Reports*, *3*(1). <https://doi.org/10.1038/srep02013>
- Dufresne, J. L., Foujols, M. A., Denvil, S., Caubel, A., Marti, O., Aumont, O., et al. (2013). Climate change projections using the IPSL-CM5 Earth system model: From CMIP3 to CMIP5. *Climate Dynamics*, *40*(9–10), 2123–2165. <https://doi.org/10.1007/s00382-012-1636-1>
- Hao, H., Ferguson, D. K., Chang, H., & Li, C. S. (2012). Vegetation and climate of the Lop Nur area, China, during the past 7 million years. *Climatic Change*, *113*(2), 323–338. <https://doi.org/10.1007/s10584-011-0347-7>
- Haywood, A. M., Dowsett, H. J., & Dolan, A. M. (2016). Integrating geological archives and climate models for the mid-Pliocene warm period. *Nature Communications*, *7*. <https://doi.org/10.1038/ncomms10646>
- Haywood, A. M., Dowsett, H. J., Robinson, M. M., Stoll, D. K., Dolan, A. M., Lunt, D. J., et al. (2011). Pliocene model Intercomparison project (PlioMIP): Experimental design and boundary conditions (experiment 2). *Geoscientific Model Development*, *4*(3), 571–577. <https://doi.org/10.5194/gmd-4-571-2011>
- Haywood, A. M., Hill, D. J., Dolan, A. M., Otto-Bliesner, B. L., Bragg, F., Chan, W. L., et al. (2013). Large-scale features of Pliocene climate: Results from the Pliocene model Intercomparison project. *Climate of the Past*, *9*(1), 191–209. <https://doi.org/10.5194/cp-9-191-2013>
- Hill, D. J., Haywood, A. M., Hindmarsh, R. C. A., & Valdes, P. J. (2007). Characterizing ice sheets during the Pliocene: Evidence from data and models. In M. Williams (Eds.), *Deep-time perspectives on climate change: Marrying the signal from computer models and biological proxies* (pp. 517–538). Geological Society, London, Special Publications, London, UK.
- Hill, D. J., Haywood, A. M., Lunt, D. J., Hunter, S. J., Bragg, F. J., Contoux, C., et al. (2014). Evaluating the dominant components of warming in Pliocene climate simulations. *Climate of the Past*, *10*(1), 79–90. <https://doi.org/10.5194/cp-10-79-2014>
- Jansen, E., Overpeck, J., Briffa, K. R., Duplessy, J.-C., Joos, F., Masson-Delmotte, V., et al. (2007). Palaeoclimate. In S. Solomon et al. (Eds.), *Climate Change 2007: The Physical Science Basis. Contribution of Working Group I to the Fourth Assessment Report of the Intergovernmental Panel on Climate Change*. Cambridge, United Kingdom and New York, NY: Cambridge University Press.
- Jiang, H., & Ding, Z. L. (2008). A 20 Ma pollen record of East-Asian summer monsoon evolution from Guyuan, Ningxia, China. *Palaeogeography, Palaeoclimatology, Palaeoecology*, *265*(1–2), 30–38. <https://doi.org/10.1016/j.palaeo.2008.04.016>
- Li, X. Q., Li, C. S., Lu, H. Y., Dodson, J. R., & Wang, Y. F. (2004). Paleovegetation and paleoclimate in middle-late Pliocene, Shanxi, central China. *Palaeogeography, Palaeoclimatology, Palaeoecology*, *210*(1), 57–66. <https://doi.org/10.1016/j.palaeo.2004.03.007>
- Li, X. Y., Jiang, D. B., Tian, Z. P., & Yang, Y. B. (2018). Mid-Pliocene global land monsoon from PlioMIP1 simulations. *Palaeogeography, Palaeoclimatology, Palaeoecology*. <https://doi.org/10.1016/j.palaeo.2018.06.027>
- Li, X. Y., Jiang, D., Zhang, Z., Zhang, R., Tian, Z., & Yan, Q. (2015). Mid-Piacenzian westerlies from PlioMIP simulations. *Advances in Atmospheric Sciences*, *32*(7), 909–923. <https://doi.org/10.1007/s00376-014-4171-7>
- Lunt, D. J., Haywood, A. M., Foster, G. L., & Stone, E. J. (2009). The Arctic cryosphere in the mid-Pliocene and the future. *Philosophical Transactions of the Royal Society of London, Series A: Mathematical, Physical and Engineering Sciences*, *367*(1886), 49–67.
- Ma, Y. Z., Wu, F. L., Fang, X. M., Li, J. J., An, Z. S., & Wang, W. (2005). Pollen record from red clay sequence in the central Loess Plateau between 8.10 and 2.60 Ma. *Chinese Science Bulletin*, *50*(19), 2234–2243.
- Meinshausen, M., Smith, S. J., Calvin, K., Daniel, J. S., Kainuma, M. L. T., Lamarque, J. F., et al. (2011). The RCP greenhouse gas concentrations and their extensions from 1765 to 2300. *Climatic Change*, *109*(1–2), 213–241. <https://doi.org/10.1007/s10584-011-0156-z>
- Miller, K. G., Wright, J. D., Browning, J. V., Kulpecz, A., Kominz, M., Naish, T. R., et al. (2012). High tide of the warm Pliocene: Implications of global sea level for Antarctic deglaciation. *Geology*, *40*(5), 407–410. <https://doi.org/10.1130/G32869.1>
- Salzmann, U., Dolan, A. M., Haywood, A. M., Chan, W. L., Voss, J., Hill, D. J., et al. (2013). Challenges in quantifying Pliocene terrestrial warming revealed by data-model discord. *Nature Climate Change*, *3*(11), 969–974. <https://doi.org/10.1038/nclimate2008>
- Salzmann, U., Haywood, A. M., & Lunt, D. J. (2009). The past is a guide to the future? Comparing middle Pliocene vegetation with predicted biome distributions for the twenty-first century. *Philosophical transactions. Series A*, *367*(1886), 189–204. <https://doi.org/10.1098/rsta.2008.0200>
- Sohl, L., Chandler, M., Schmunk, R., Mankoff, K., Jonas, J., Foley, K., & Dowsett, H. (2009). *PRISM3/GISS Topographic Reconstruction: US Geological Survey Data Series 419*. Reston, Va: U.S. Geol. Surv.
- Sun, Y., Ramstein, G., Contoux, C., & Zhou, T. J. (2013). A comparative study of large-scale atmospheric circulation in the context of a future scenario (RCP4.5) and past warmth (mid-Piacenzian). *Climate of the Past*, *9*(4), 1613–1627. <https://doi.org/10.5194/cp-9-1613-2013>
- Sun, Y., Zhou, T. J., Ramstein, G., Contoux, C., & Zhang, Z. S. (2016). Drivers and mechanisms for enhanced summer monsoon precipitation over East Asia during the mid-Pliocene in the IPSL-CM5A. *Climate Dynamics*, *46*(5–6), 1437–1457. <https://doi.org/10.1007/s00382-015-2656-4>
- Wu, F., Fang, X., Ma, Y., Herrmann, M., Mosbrugger, V., An, Z., & Miao, Y. (2007). Plio-quaternary stepwise drying of Asia: Evidence from a 3-Ma pollen record from the Chinese loess plateau. *Earth and Planetary Science Letters*, *257*, 160–169.
- Wu, Y. S. (2001). Palynoflora at late Miocene-early Pliocene from Leijihae of Lintai, Gansu Province, China. *Acta Botanica Sinica*, *43*, 750–756.
- Yao, J. C., Zhou, T. J., Guo, Z., Chen, X. L., Zou, L. W., & Sun, Y. (2017). Improved performance of high-resolution atmospheric models in simulating the East Asian summer monsoon rain belt. *Journal of Climate*, *30*(21), 8825–8840. <https://doi.org/10.1175/JCLI-D-16-0372.1>
- Zhang, R., Jiang, D., & Zhang, Z. (2015). Causes of mid-Pliocene strengthened summer and weakened winter monsoons over East Asia. *Advances in Atmospheric Sciences*, *32*(7), 1016–1026. <https://doi.org/10.1007/s00376-014-4183-3>

- Zhang, R., Yan, Q., Zhang, Z. S., Jiang, D., Otto-Bliesner, B. L., Haywood, A. M., et al. (2013). Mid-Pliocene East Asian monsoon climate simulated in the PlioMIP. *Climate of the Past*, 9, 2085–2099.
- Zhang, Y. G., Ji, J. F., Balsam, W., Liu, L. W., & Chen, J. (2009). Mid-Pliocene Asian monsoon intensification and the onset of northern hemisphere glaciation. *Geology*, 37(7), 599–602. <https://doi.org/10.1130/G25670A.1>
- Zhang, Z., Nisancioglu, K. H., & Ninnemann, U. S. (2013). Increased ventilation of Antarctic deep water during the warm mid-Pliocene. *Nature Communications*, 4(1), 1499. <https://doi.org/10.1038/ncomms2521>
- Zhao, L.-C., Collinson, M. E., & Li, C.-S. (2004). Fruits and seeds of *Ruppia* (Potamogetonaceae) from the Pliocene of Yushe Basin, Shanxi, northern China and their ecological implications. *Botanical Journal of the Linnean Society*, 145(3), 317–329. <https://doi.org/10.1111/j.1095-8339.2003.00278.x>